

## The slip surface mechanism of delayed failure of the Brumadinho tailings dam in 2019

Fangyuan Zhu<sup>1</sup>, Wangcheng Zhang<sup>1,2</sup> & Alexander M. Puzrin<sup>1</sup>  

The 2019 Feijão dam failure in Brumadinho, Brazil, claimed 270 lives and caused enormous environmental damage. A special feature of this failure was that it took place three years after the tailings disposal was terminated, which should have allowed sufficient time for the material to consolidate and increase its strength. Here we propose a basic physical mechanism of a delayed slip surface growth along weak layers of fine tailings within the dam body. Using accurate numerical modelling of all stages of the evolution of the Feijão dam, we show how this growth was preconditioned by dam construction and tailings discharge history and further driven by creep deformation during the post-closing stage, until the slip surfaces reached their critical length, resulting in their unstable propagation and the rapid collapse of the entire dam. Main factors controlling the time of failure have been identified, facilitating future risk assessment for decommissioned tailings dams.

<sup>1</sup>Institute for Geotechnical Engineering, ETH Zürich, Stefano-Francini-Platz 5, 8093 Zürich, Switzerland. <sup>2</sup>Department of Engineering, Durham University, Lower Mount Joy, South Road, Durham DH1 3LE, UK. ✉email: [alexander.puzrin@igt.baug.ethz.ch](mailto:alexander.puzrin@igt.baug.ethz.ch)

On 25<sup>th</sup> January 2019, a tailings dam at the Córrego do Feijão iron ore mine, in the Brumadinho city, Brazil, failed suddenly, killing 270 people and seriously affecting the regional ecosystem<sup>1–3</sup>. The Brumadinho dam disaster occurred just three years after the failure of the Fundão dam located around Mariana city in the same state<sup>4,5</sup>. The collapse of these tailings dams, both owned by the mining company Vale, resulted in tightened regulations for operating dams and the commitment from the Brazilian government of decommissioning all upstream mining dams<sup>4</sup>.

Mining products are widely used in modern manufacturing of, e.g., computers, smart devices, airplanes, jewellery etc., and in many developing countries the mining industry is dominant in the economy, playing an important role in removing poverty and creating job opportunities<sup>6</sup>. Tailings, which are waste products of the beneficiation process, are usually deposited in a pond and protected by a tailings dam<sup>7</sup>. With the rapid growth of the mining activities, incidents of tailings dam failure have occurred frequently, with five to six catastrophic cases reported annually on a global scale after 2000<sup>8–10</sup>. Failure of a tailings dam can be caused by multiple environmental and human factors such as increased loading by rapid tailings discharge, earthquakes, rainfalls and weak dam foundations<sup>11–14</sup>. It is of great importance to understand the dominant triggering factors of failed tailings dams such as the Brumadinho dam to effectively avoid failure recurrence in the same region.

Figure 1 shows the location and extent of the Brumadinho dam disaster. The failure extended across the face of the dam and released 9.7 Mm<sup>3</sup> of stored tailings with the mudflow running through the Paroepaba River<sup>15,16</sup> and demolishing infrastructure that it came across, including a canteen where miners were having lunch. The failure occurred without any notification, despite the fact that the dam had stopped receiving tailings since 2016 and been equipped with state-of-the-art monitoring instrumentation<sup>17</sup>. Geotechnical reports prior to the failure indicated the dam was on a safe side. Despite its scale and impact, as well as the considerable effort invested into its investigation, the cause of the failure remains debated, mainly due to its delayed nature. The expert panel, appointed by Vale after the disaster, suggested that the failure was associated to the internal creep and the loss of suction induced by heavy rainfall at the end of 2018<sup>18</sup>. In contrast, the report of the Federal Police of Brazil concluded the disaster was triggered by vertical perforations in a weak point of the dam structure, which was supported by Arroyo and Gens<sup>19</sup>. The resulting uncertainty may impede avoiding similar tragedies in the future.

This study presents a mechanism in which failure is initiated within layered fine tailings or slimes beneath upstream constructed dams and followed by a slow slip surface growth, first driven by the increasing weight of the deposited tailings and then, after the dam closure, by the creep deformations. While other

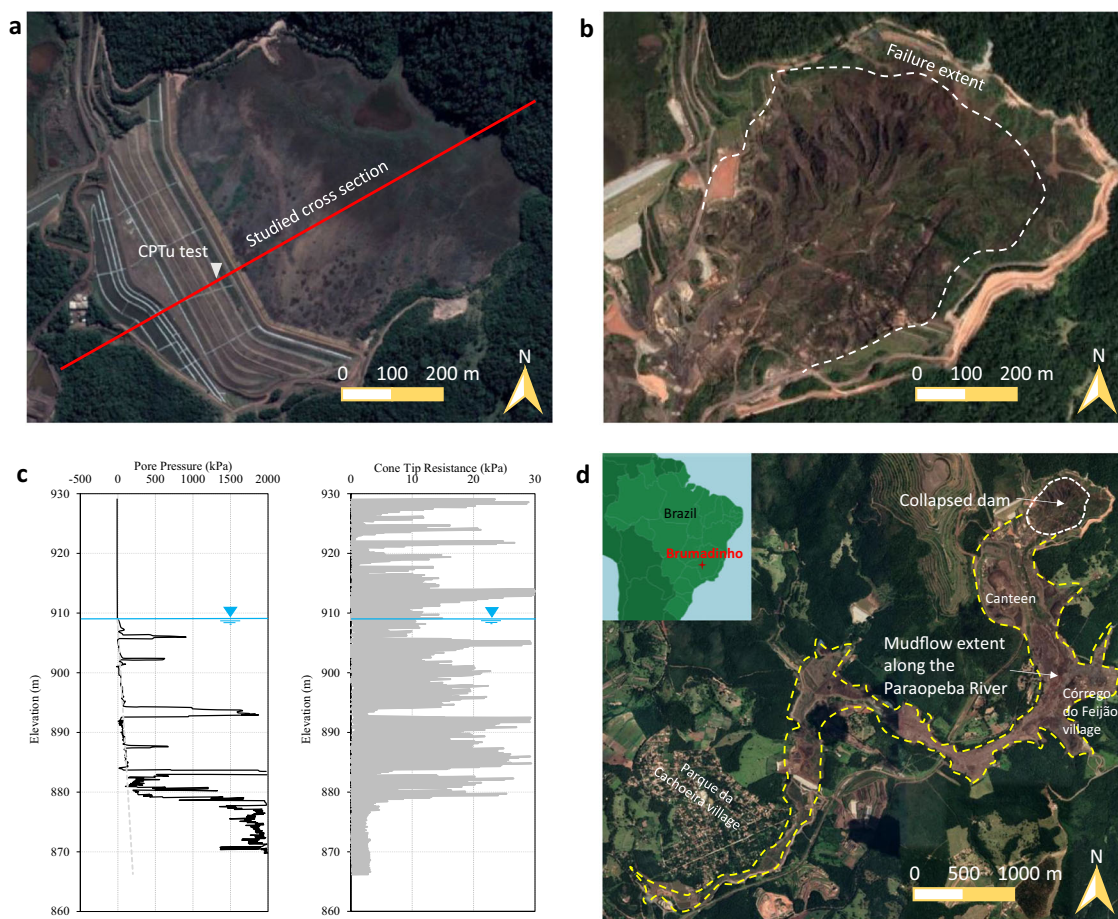


**Fig. 1** Satellite images taken before and after the Brumadinho tailings dam failure and geotechnical cone penetration test (CPTu) data prior to failure. **a** Image of the Feijão dam prior to failure, studied cross-section and location of CPTu test. (Source: Google Earth 3D, image dated June 30, 2018) **b** Post-collapse image of the Feijão dam. (Source: Google Earth 3D, image dated July 30, 2022) **c** Profiles of pore pressure and tip resistance from the CPTu test showing the distribution of interlayered fine tailings layers (after<sup>18</sup>). **d** Map showing the dam location and impact area of the tailings mud flow. (Source: Google Earth 3D, image dated July 30, 2022). Note: Historical images of the dam were retrieved using the Google Earth Pro with the specific coordinates of 20°07'12.05" S latitude and 44°07'14.55" W longitude.

triggers such as rainfall and borehole drilling could have accelerated the slip surface growth, we demonstrate that creep alone would be sufficient for the slip surface to reach the critical length, making the catastrophic failure inevitable. This is a worrying outcome for existing dams, where tailings exhibit brittle and rate-dependent behaviour: the absence of unfavourable environmental and human factors does not guarantee long-term dam safety.

## Results

The entire evolution of the Feijão dam from the gradual upstream construction and operation to the post-closure phase followed by dynamic catastrophic failure was investigated numerically using a large deformation finite element scheme. The main assumptions and results are provided below followed by discussion of the physical mechanism and controlling factors. The numerical procedure and analytical criteria are briefly described in the Methods section.

### Properties of tailings and their implications for the Feijão dam failure.

The main three features of the tailings behaviour contributing to the dam collapse are (i) their brittle structure, (ii) creep and (iii) segregation into coarser and finer layers during their deposition. Tailings stored within the Feijão dam were produced from the Córrego do Feijão iron ore mine, and their iron content often exceeds 50%<sup>15,20</sup>. The iron oxidation built between tailings particles can effectively act as cementitious bonds, which was observed through scanning electron microscopic images (Fig. 2a). During shearing, the interparticle bonding structure may collapse in a brittle manner resulting in the reduction of material strength from peak towards residual, i.e., strain softening. Meanwhile, the loose and saturated tailings

behave contractive at large strains producing excess pore pressures, further deteriorating the tailings' resistance against loading. Sometimes, the generated pore pressures become so large that the load transferred to the tailings particles practically vanishes, leading to the so-called 'static liquefaction'<sup>21,22</sup>. Advanced laboratory testing and in-situ CPTu data confirmed the brittle strength loss (see Fig. 2b, c) in the Feijão dam tailings. The brittle nature of tailings facilitates a rapid failure process resulting in the undrained condition during any local failure, because the generated excess pore pressure does not have sufficient time to dissipate via seepage. This phenomenon is critical for understanding the undrained character of the slip surface growth.

Another important physical phenomenon relevant for understanding the delayed failure of the Feijão dam is creep<sup>23</sup>. Laboratory tests showed that the Brumadinho iron ore tailings tend to deform continuously under constant stresses, with some of the tailings particles changing their positions and corresponding force chains rearranging to accommodate the external loads. As seen in Fig. 2d, the creep rate increases with the applied stress. The presence of fine particles in loose tailings also increases the creep rate. The strains accumulated due to creep are particularly dangerous when combined with the brittle tailings behaviour, because they can cause the growth of slip surfaces at constant loads, resulting in a delayed failure even if a tailings dam is in the postclosing phase without further discharge of tailings. The influence of creep in the failure of the Feijão dam will be evaluated through numerical analyses by incorporating an advanced creep constitutive model.

Finally, the segregation of the tailings during their deposition into coarser and finer layers is another critical aspect in the Feijão dam failure analysis<sup>24</sup>. According to the position of a new raising to relative previous raisings, there are three types of dam

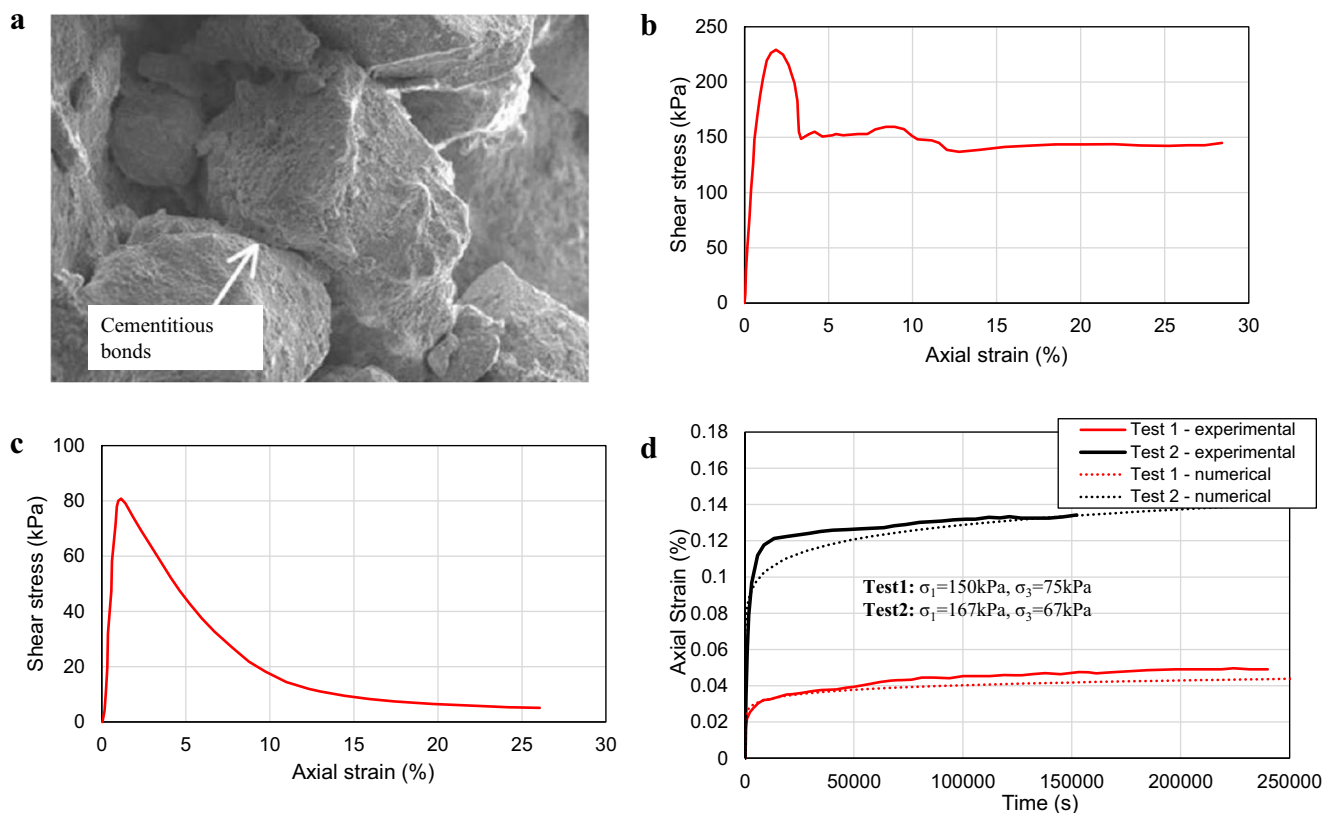


**Fig. 2 Mechanical behaviour of Brumadinho tailings (after<sup>18</sup>).** **a** Scanning electron microscope of tailings. **b** Stress-strain relationship under a drained triaxial test (confining pressure: 100 kPa). **c** Stress-strain relationship under an undrained triaxial test (confining pressure: 100 kPa). **d** Creep strain under sustained load.

raises: upstream, centreline and downstream. The Feijão dams was built in the upstream manner, where trapezoidal embankments are constructed toe to crest of another, moving the crest further upstream (see Fig. 3a). The upstream raising technique requires deposition close to the dam of a free-draining beach of coarse tailings, with fine tailings and slimes deposited further away from the crest. This natural division enables relatively safe construction of the new dam on the sand beach from a previous raising. However, controlled by the discharge rate, tailings properties, internal drainage settings, etc., the length of a drained sand beach often varies between different raisings and fine tailings might be deposited close to the crest of previous dams. This leads to the formation of fine tailings layers within the coarse beaches, which have to sustain the load from the upper dams<sup>25</sup>. For the Feijão dam, the presence of fine tailings beneath dams becomes even more evident after the fourth raising (see Fig. 3a), where the set-back had to be implemented in order to reduce the slope gradient. This layered structure feature was confirmed through an in-situ cone penetration test (CPTu) under the eighth dam, as shown in Fig. 1c. The profiles of resistance and pore pressures obtained from the CPTu test revealed that the materials are composed of interlayered coarse and fine tailings. As will be shown in the study, the presence of fine tailings under dams facilitated the initiation of the failure and the layered structure offered a locus for the subhorizontal failure propagation.

**The mechanism of slip surface growth.** In general, a shear failure in solid materials rarely takes place simultaneously along the entire final shear surface, initiating instead in a limited portion, with subsequent propagation under either increasing or constant external loads. For continuous solid materials exhibiting brittle behaviour, this phenomenon is often referred to as a shear crack propagation and can be analysed using fracture mechanics<sup>26,27</sup>. For a particulate system, however, such as an earth dam composed of strain-softening iron ore tailings, it manifests itself as a slip surface growth, which can be either progressive (steady-state), requiring increasing external loads, or catastrophic (unstable), under existing external loads<sup>28–32</sup>. At a certain limit, progressive slip surface growth can evolve into the catastrophic failure, the criteria for which have been discussed in Zhang et al.<sup>33</sup>.

In the Feijão dam case, the fine tailings layers within the coarse sand beach (Fig. 3a) provided the locus for the slip surface. Our working hypothesis, schematically shown in Fig. 3b, is that the initial slip surface has likely initiated within one or several of these fine layers and propagated progressively under the increasing weight of the dam during its construction. The length of the slip surface within the weaker fine layers was not, however, sufficient to cause the catastrophic failure of the dam during and immediately after its construction. Since no more tailings were deposited, the weight of the dam stopped increasing and the slip surface should have stopped growing

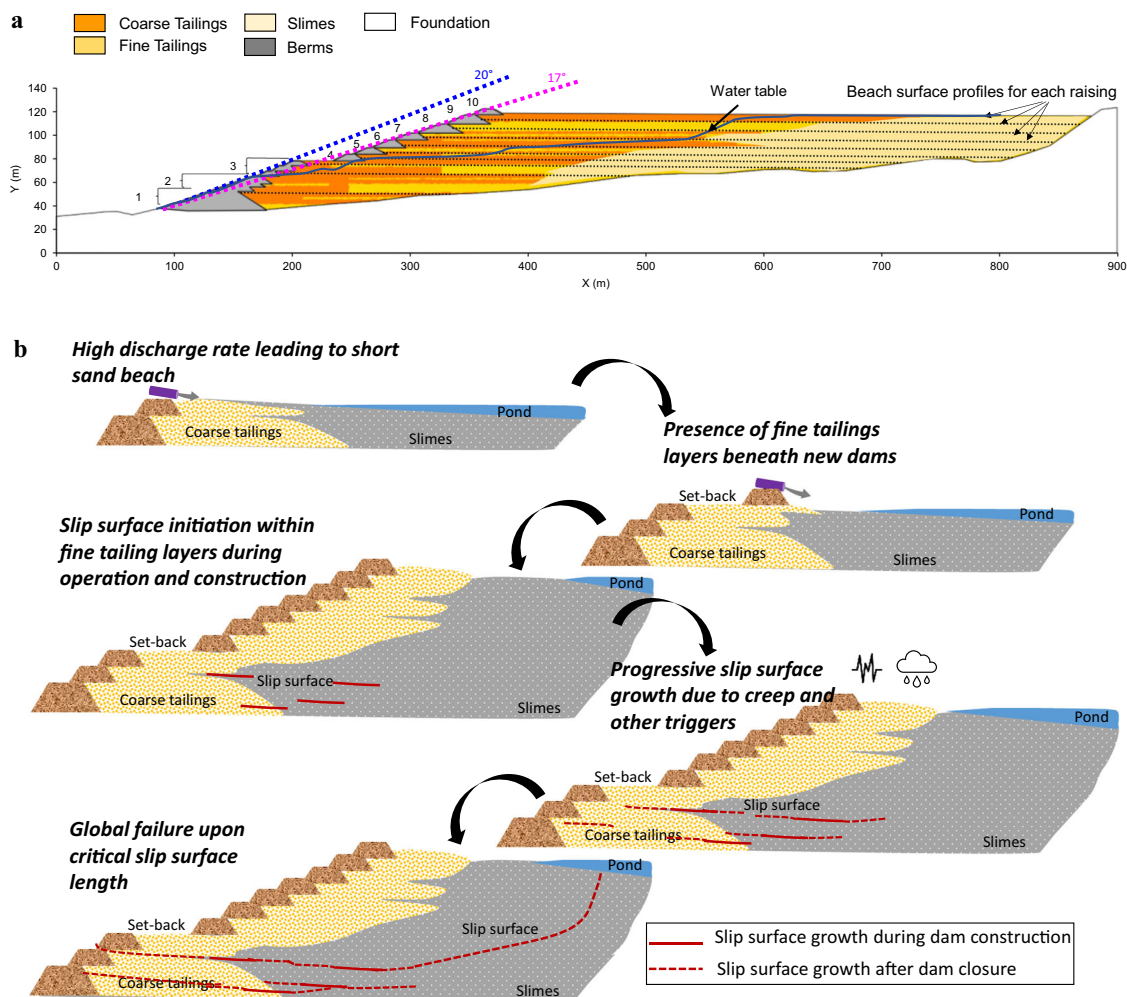


**Fig. 3** Slip surface growth mechanism for the Feijão dam failure. **a** Layout of raisings and layering of tailing in the Feijão dam; **b** Initiation and propagation of slip surfaces during the dam construction/operation and after the closure.

progressively, i.e., its critical length necessary for the onset of the unstable catastrophic propagation could never be reached. Nevertheless, the dam failed.

We propose a mechanism of a delayed catastrophic failure of the Feijão dam (Fig. 3b), where after the dam closure, the slip surfaces continued growing within the fine tailings layers under the constant external loads, driven purely by the creep deformations. This growth was very slow, due to the slow creep rates, and yet unstable, since no increase in external forces was required. This slow process continued, until the length of the slip surface has reached the critical value, triggering the classical catastrophic slip surface propagation and subsequent dam failure. The proposed mechanism will be validated and discussed in the following sections.

**Slip surface initiation and growth during the dam construction and operation.** The dam consists of 10 raises with the starter dam completed in 1976 and tailings disposal ceased in 2016. Raises are schematically illustrated in Fig. 4a. The height of raises varies between 5 to 18 m, with the total height from the toe to the crest being 86 m and the final crest elevation being 942 m above the sea level.

The slope angle of the first three dams was designed to be 20° to horizontal but adjusted to 17° after the fourth raising through construction of a setback (Fig. 4a). According to our numerical modelling, the initial design is not conservative and without the setback the Feijão dam should have collapsed at the sixth raising, with failure initiating from the toe. While the improvement of the centreline saved the dam, it also moved the upper portion of the dam closer to the pond and above fine tailings layers, which offered conditions for progressive growth of slip surfaces inside the Feijão dam (Fig. 4b).

The average discharge rate of tailings was about 2.3 m/y, with a total height of 87 m in 37 years that would result in an excess pore pressure ratio of around 0.01 (water takes 1% of load) based on the Gibson's solution<sup>34</sup>, which in principle indicates drained conditions. However, often the local discharge rate is much higher than the average value considering interruption by

operational maintenance and dam construction, which may lead locally and temporarily to practically undrained conditions. This can result in a local failure with strain softening, irreversibly changing the strength of tailings, even after the excess pore water pressures have dissipated and locally failed tailings consolidated under the new load. In this study, the rapid undrained discharge with the subsequent slow increase in shear strength due to consolidation will be our main working hypothesis. The effects of an alternative assumption, of a slow drained discharge, on the mechanism and time to failure are presented later in the Discussion section.

Our rigorous numerical modelling allowed for capturing the stress history during the continuing raising of the dam and discharge of tailings (see Fig. 4b). The localized plastic deformation first becomes evident at the seventh raising, with the initiation of slip surfaces No. 1, 2 and 3. With further elevation of the dam, the plastic regions grow as a result of the continuing discharge of tailings, with slip surface 1 daylighting at the dam surface at the eighth raising and the new slip surface No. 4 nucleating at the ninth raising. Inspection of Fig. 4b shows that the localized failure is mainly concentrated within the regions dominated by fine tailings because of their lower shear strength. Despite the local plastic deformation, the dam remains globally stable after the completion of all ten raisings, which is in alignment with the design and consistent with observations. However, this plastic shearing significantly weakens the tailings at the slip surfaces, pre-conditioning these localized shear zones towards further growth that will eventually cause the Brumadinho disaster.

**Creep-driven slip surface growth after the dam closure.** Risk assessment of tailings dams commonly focuses on the construction and operation phase when the load increases fast with the discharge of uncompacted tailings slurry. With long-term consolidation, tailings become compacted with the formation of iron ore bonding structure, gaining strength and hence reducing risk of a slope failure. Therefore, a closed dam is supposed to be on a safe side compared to the one receiving tailings discharge, unless

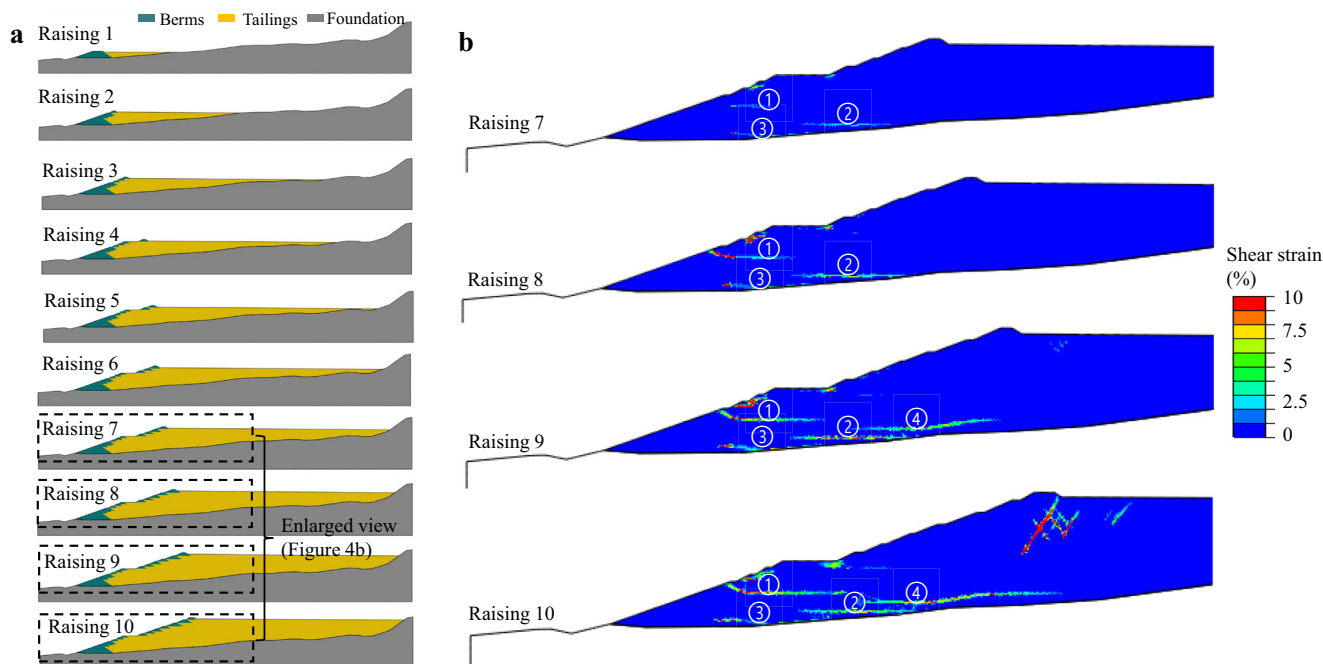


**Fig. 4 Numerical modelling of the construction and operation stage.** **a** Layouts of dams and tailings for ten raises. **b** Distributions of accumulated total shear strain at raisings 7–10.

it is subjected to external factors like earthquakes or exceptionally strong precipitation combined with inefficient drainage conditions leading to piping<sup>35</sup>. There was, however, no significant seismic shaking or evidence of piping reported prior to the Feijão dam collapse. Instead, we believe that an internal failure mechanism was in motion, turning the Feijão dam into a “ticking time bomb”.

The dam maintained almost the same post-closure effective stress level for two and a half years before the collapse. Nevertheless deformations of the dam continued, driven by creep first at a faster and then at a slower rate. Figure 5a provides measured displacement of the dam surface in the year prior to the failure (2018-2019), available from the satellite images and compares them to the surface displacements predicted

numerically for the same period. Using the creep model described in Methods resulted in a rather close prediction of the observed displacement at the slope of the dam and its crest, below which the main slip surfaces have been growing. Further away from the crest, the model underestimates the settlements of the dam surface, likely caused by a long-term consolidation, which was not accounted for in the model due to its minor effect on the slip surface growth.

Creep is a long-term process ensuring dissipation of any generated pore pressure and hence the drained conditions. However, at the tip of a slip surface the creep deformation is likely to cause a rapid brittle failure of tailings (as indicated in Fig. 2b, c), which in combination with the lower permeability of fine-grained tailings indicates that the growth of the slip surface is

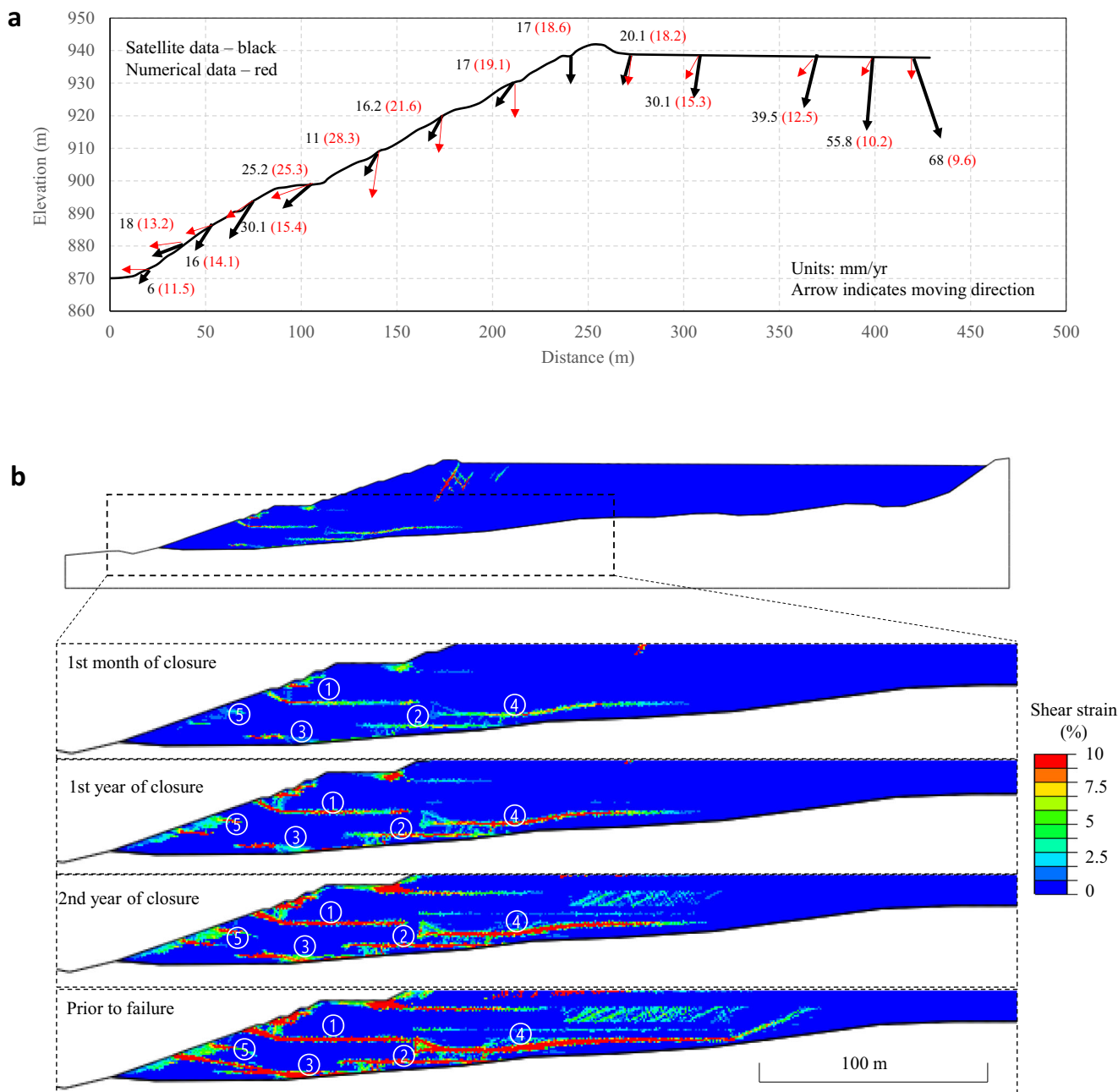


**Fig. 5 Numerical modelling of the post-closure stage. a** Annual displacement in 2018-2019 obtained from numerical modelling compared to the satellite image analysis (after<sup>18</sup>). **b** Creep performance of tailings dam after the closure of the Feijão dam: total shear strain with unfavored undrained discharge history.

likely to take place under undrained conditions. Indeed, as observed from our numerical modelling, the main slip surface grows post-closure at a rate as high as 40 cm/day. In reality, this growth is not a continuous process but a sequence of discrete propagation events taking place at even higher velocities, where a rapid propagation of the slip surface tip is accompanied by equally fast shearing along the entire slip surface. Note, that assumption of undrained conditions represents an unfavourable scenario.

Numerical modelling of the dam construction reveals that multiple slip surfaces have already been formed after the completion of ten raisings mainly ranging between the starter and the fourth dams with elevation from 870 m to 900 m (surfaces No. 1, 2, 3 and 4 in Fig. 4b). Figure 5b shows the plastic strains accumulated due to creep at different times prior to the failure. A number of new slip surfaces are initiating due to creep within the first month after the closure, with the slip surface No. 5 being of particular interest for the future analysis. Continuing creep displacements help to overcome the peak strength of tailings at the slip surface tips, causing the growth of slip surfaces. At the end of 2018, the gap between the slip surfaces No. 1 and 4 is almost closed, with the second set of slip surfaces located 10 m deeper (No. 2, 3 and 5), also merging together. Delay in these mergers was influenced by the need to cut through the layers of course material separating the surface tips.

#### Reaching the critical length for a catastrophic propagation.

From the numerical modelling (Fig. 5b) it can be concluded that the catastrophic slip surface growth commenced when the combined length of the top two surfaces (No. 1 and 4) reached about 250 m. This result can be validated using the analytical criterion for the onset of catastrophic slip surface growth in a cut planar slope proposed by Zhang et al.<sup>36</sup>. The corresponding analysis has been carried out in the Methods section. It follows that for the two slip surfaces No. 1 and 4 located at the average depth of 60 m, the critical length is about 200 m. This explains why their merger and subsequent growth to the combined length of 250 m served as a trigger of their unstable propagation leading to the collapse of the dam. Similar analysis was carried out for the bottom three surfaces (No. 3, 4, and 5 in Fig. 5b) which were also merging at the onset of the failure. The critical length of a slip surface at the depth of these three surfaces (averaged at 70 m) is 210 m, which is larger than their combined length of 140 m prior to failure. This is consistent with the observation that the catastrophic slip surface growth takes place after the merging of the top two surfaces rather than of the three bottom ones.

**Catastrophic dam collapse.** Figure 6 shows the simulated dynamic behaviour at the onset of collapse compared to the actual video footage. Within half a second from the onset of its catastrophic propagation, the main slip surface in Fig. 5b daylighted at the dam surface above the starter dam. This is consistent with the high-quality video images of the event where an obvious bulge can be recognised above the starter dam. The consistency of the predicted deformation pattern at the onset of failure with observations confirms that the ‘weak’ fine tailings layer present above the first raising (Fig. 1c), where the slip surface No. 1 had initiated, played a critical role in the formation of the failure mechanism. Within the following five seconds the main slip surface propagates upwards to the bottom of the pond, about 300 m behind the crest of the dam. This causes the sinking of the crest and sets in motion enormous volumes of saturated tailings, shearing and liquefying them. Comparing in Fig. 6 field maps of displacements at 6.7 s and 11 s provides evidence of retrogressive failure, which gradually removes more tailings upslope. The

purpose of the presented sophisticated and computationally expensive dynamic modelling has been to illustrate the mechanism of transfer from delayed slip surface growth to the catastrophic failure, which occurred within the first eleven seconds after the main slip surface had reached the critical length. The subsequent runout behaviour of liquefied tailings can be more efficiently simulated by numerically solving the depth-averaged shallow water equations or by using an agent-based model, which have been studied in some recent publications<sup>37,38</sup>.

#### Discussion

In the numerical simulations, the transfer from the progressive to the catastrophic slip surface growth was driven solely by creep under practically constant load and did not require any external trigger. At the same time, it has been shown that the delayed propagation of the slip surfaces prior to failure, resulted in rather small displacements observed at the surface of the dam (about 30 mm over the last year before failure). This probably explains why there was no obvious deformation identified prior the collapse of the Feijão dam.

**Time to failure.** Figure 7a presents the growth of the main slip surface after the closure of the dam. During the first year after the closure, the slip surface grows impressive 130 m due to the higher initial creep rate. The creep rate decreases with time and hence the propagation of slip surface decelerates after the first year with the length increased by 50 m over the following two years, corresponding to a stable growth stage. After 32 months and prior to the failure, the slip surface saw a fast propagation due to the merging of the two slip surfaces.

In real life the time to failure is influenced by multiple factors, such as the construction and operation history, post-closing creep rate, environmental loads etc, and is therefore difficult to predict in practice. Nevertheless, the advanced numerical modelling presented above has been capable of correctly predicting the failure three years after the closure of the dam. This demonstrates that a lifecycle numerical modelling using an advanced constitutive model of tailings has a potential to serve as an effective tool to identify delayed internal propagation of slip surfaces that can be hardly detected via the state-of-the-art site monitoring tools. The prediction of sudden catastrophic failure can be made by conducting the numerical investigation of the type performed in this study.

**Effects of discharge history.** Another advantage of the advanced lifecycle numerical modelling lies in its ability to conduct efficient parametric studies towards a better understanding of the controlling factors for the time to failure. This can facilitate the choice of proper mitigation measures to avoid the catastrophic failure. Usually, the discharge rate varies over the course of the operation phase with the rate normally averaged between ~10,000 and ~100,000 tonnes per day. Often, the rate varies between locations. For example, the discharge process is interrupted when a portion of the dam is under construction and more tailings need to be discharged elsewhere. This leads to a locally rapid loading of tailings slurry resulting in undrained conditions during the discharge period, and the time to failure obtained by the numerical modelling considering this discharge interruption agrees well with the observations. If this construction/operation history was neglected, the loading would have to be modelled under drained condition, resulting in the plastic deformation occurring mainly near the starter dam and forming a curved slip surface (Fig. 7b), which does not, however, result in a dam collapse. The fine tailings layers remain intact because the load by tailings discharge under drained conditions causes increase in shear strength.

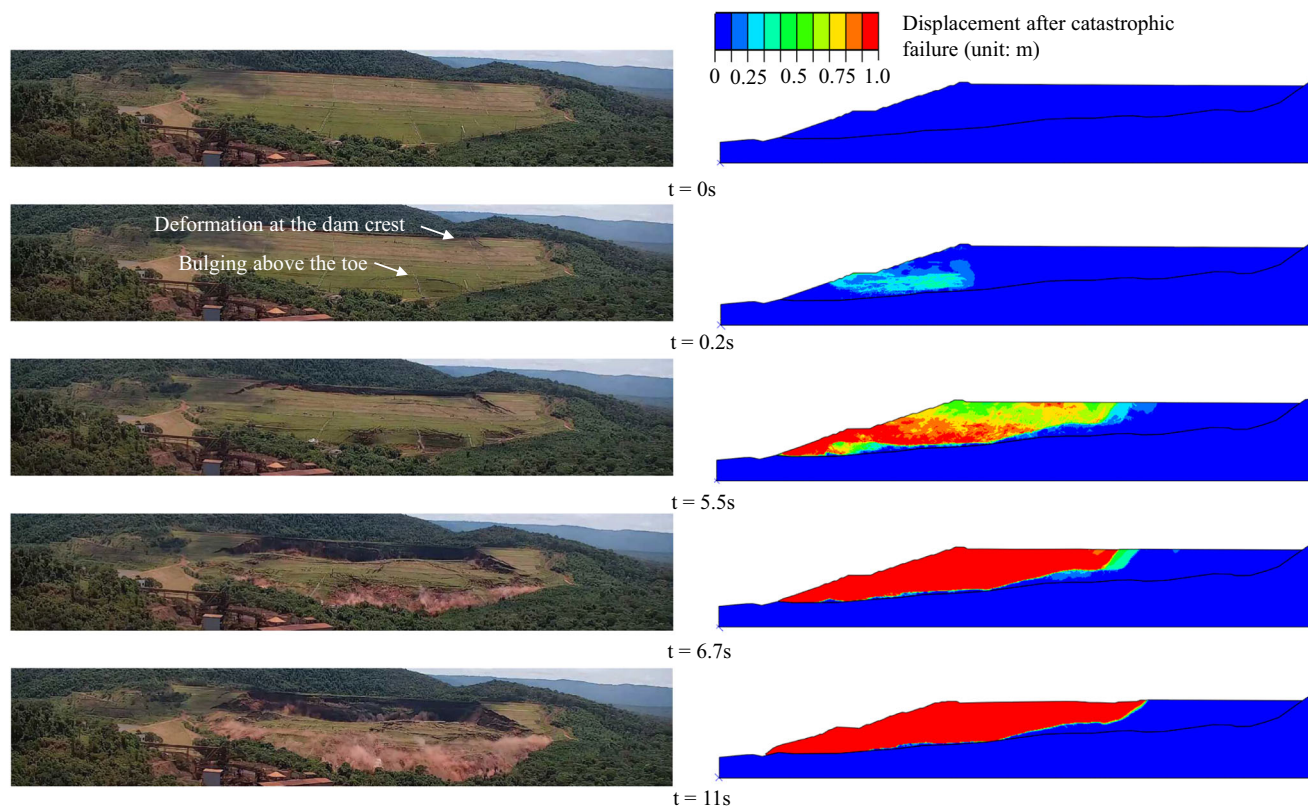


**Fig. 6 Displacement evolution at the initial stage of the catastrophic failure.** Video snapshots (on the left, after<sup>18</sup>) are printed against the results of numerical modelling (on the right), for the same elapsed times after the dynamic failure initiation.

Significantly, the delayed slip surface growth in the weak fine tailings layers is still active during the post-closing stage, but the catastrophic failure takes place later than for undrained discharge as illustrated in Fig. 7a.

**Effects of the creep rate.** Parameters of the constitutive model describing the creep behaviour have been determined using the regression analysis by fitting experimental data with the Prony series. Two creep tests with different constant stresses were conducted by the panel<sup>18</sup>, with the results shown in Fig. 1d. From our analysis it follows that the test with the at-rest earth pressure coefficient  $K_0 = \sigma_3/\sigma_1 = 0.5$  (i.e. the one with the lateral stress  $\sigma_3 = 75$  kPa and the vertical stress  $\sigma_1 = 150$  kPa) is closer to the loading conditions of the Feijão dam. It is noted, however, that the value of  $K_0$  slightly varies between different regions within the dam. If the experimental data with  $K_0 = 0.4$  ( $\sigma_3 = 75$  kPa and  $\sigma_1 = 167$  kPa) were used to generate the Prony series for the creep model, the dam would collapse in January 2017, i.e., half a year after the cease of the dam operation. The corresponding slip surface growth is illustrated as the red dashed line in Fig. 7a, indicating an extent to which the time to failure is affected by the creep characteristics of tailings.

**Effects of tailings brittleness.** In addition to the creep rate, the slip surface growth largely depends on the brittleness of the tailings. Tailings happen to be more brittle with a higher iron content, resulting in higher pore pressure accumulation during shearing. Laboratory tests show the required strain for reducing the strength to the residual state is between 4% and 10%, with a median value of around 6% used in our analysis for the base case. The numerical modelling shows that the failure might have already occurred two months after the dam closure (i.e., in 2016) if the residual strain was 4%, but might never occur with the

residual strain of 30% as indicated as the black dashed line in Fig. 7a.

**Effects of a rainfall and vertical perforations.** The creep rate decays under a constant load, so that delayed failure becomes less probable with the increase of the lapsed time. The numerical modelling shows that the annual creep strain will become less than 0.1% after 100 years, which implies a negligible annual growth of the slip surface. Therefore, if in the first few years the slip surface length has not reached the critical value for catastrophic propagation, the subsequent failure of the dam is highly unlikely. However, the slip surface growth can get reactivated when the applied load is increased or the shear strength is reduced due to, e.g., rainfalls or seismic shaking. Estimating the critical length using the criterion provided in the Methods and comparing it with the final slip surface length due to creep would allow for assessing how much safety remains in the dam and whether external factors such as extreme precipitations and seismicity should be of concern.

Site investigations show that the phreatic line generally drops with time though the dropping rate turns small during the rain seasons. This can also be confirmed by the shrinkage of the pond visible in satellite images. The change in the phreatic line after the closure of the dam was not accounted for in the numerical modelling where the highest water table level at the end of the operation was used representing the most dangerous scenario. However, since the dam collapsed during the rainy season, we modelled the loss of matric suction<sup>39</sup> for the tailings above the phreatic line and found that the tailings at the surface have little effect on the deep-seated slip surface growth. Nevertheless, the loss of suction of shallow tailings facilitates rapid development of multiple shear bands when the slip surface length reaches its

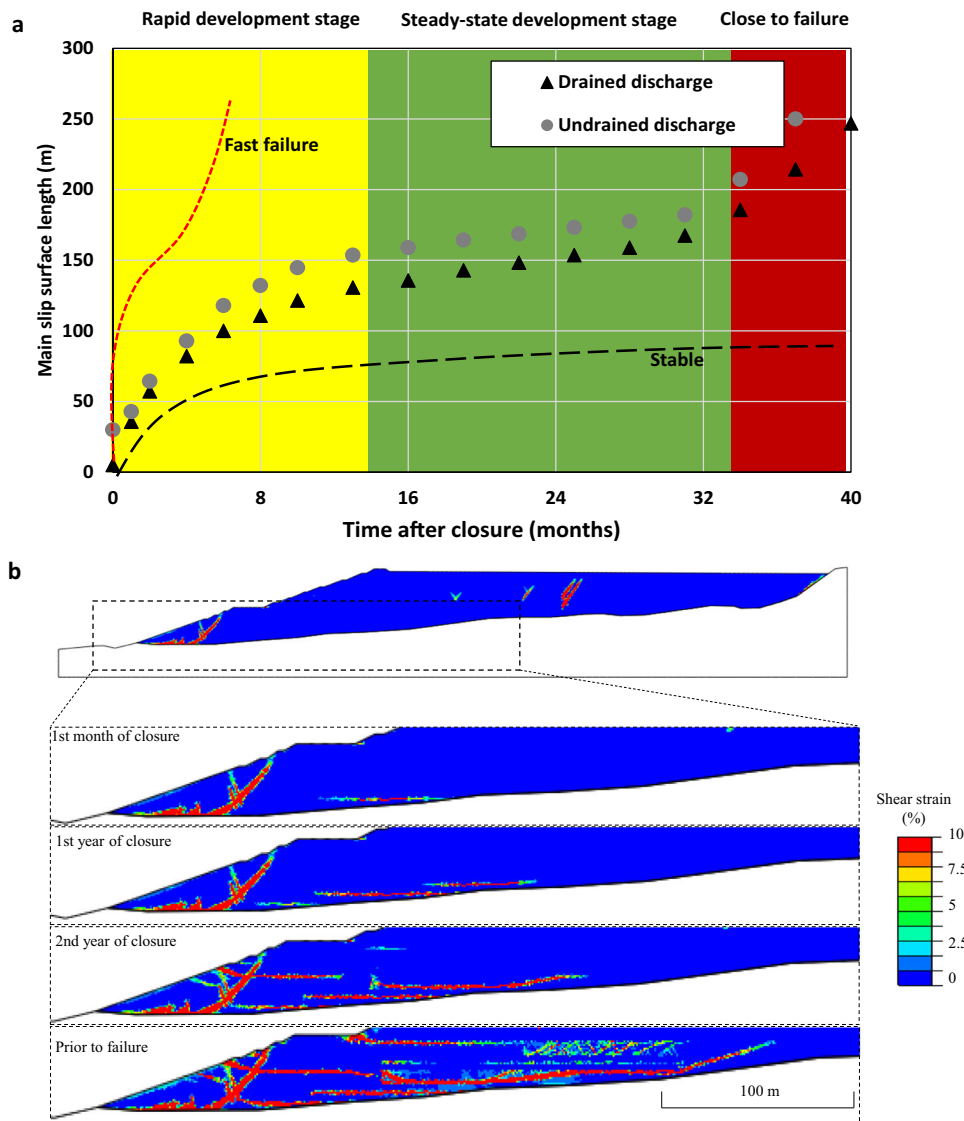


**Fig. 7 Time to failure and effects of discharge history.** **a** Growth of the main slip surface. **b** Creep performance of tailings dam after the closure of the Feijão dam with favoured drained discharge history.

critical value and contributes to the static liquefaction of the entire dam body once it sets into motion.

In addition to recorded rainfalls, some ongoing construction works, including vertical perforations, took place on-site prior to the event. While the proposed here mechanism predicts that the creep alone would be sufficient for the slip surface to reach its critical length, it does not exclude that other disturbances could have served as the last straw.

In summary, our numerical and analytical modelling indicates that the Brumadinho catastrophe can be explained by the creep-driven slip surface growth, although some negative contribution of other external triggers cannot be excluded. This mechanism is relevant for all existing dams using the upstream construction, where initial deep-seated slip surfaces may have developed during construction and operation and keep growing after closure without causing large displacements on the dam surface in the last months prior to failure. Although some mining companies, e.g., Vale, that is the owner of the two recent collapsed dams in Brazil, have committed to remove all upstream dams, their full decommissioning is unlikely to be completed before the middle of the century.

For ductile tailings, it is possible for a dam to undergo significant deformation prior to reaching a state of failure. In such instances,

monitoring surface displacement can be an effective precursor indicator. In contrast, when dealing with tailings that fail in a brittle manner, the relationship between surface displacement and dam failure is not as straightforward. Slip surface growth can occur with limited deformation, leading to surface displacements, which may not look critical. It seems that numerical modelling of the whole-life evolution of the type performed here for the Feijão dam is currently the only available tool for the risk assessment of upstream dams potentially facing the same type of failure. If the failure is possible, it can provide prediction of the time to failure and facilitate decision-making with respect to mitigation measures. If the failure due to creep alone is impossible, it can be combined with the proposed analytical criterion for the critical length of the slip surface to determine the long-term safety of the dam with respect to potential external triggers.

**Methods**

**Numerical modelling of the Feijão tailings dam life cycle.** The modelling of the Feijão dam life cycle was carried out using a large deformation finite element method with remeshing and interpolation technique<sup>36</sup>, covering the initial dam construction, ongoing operation and raisings, post-closure dam evolution, culminating with the dam failure process. The approach falls

within the category of the ‘arbitrary Lagrangian-Eulerian’ method<sup>40</sup>. It divides the whole large-deformation analysis into a series of small deformation analysis increments of finite strain elasto-plasticity<sup>41</sup>, followed by remeshing based on updated geometry and interpolation of all field quantities from old to new meshes. Lagrangian calculations were undertaken by the commercial package ABAQUS<sup>42</sup> while remeshing and interpolation of field quantities were performed in Python. Figure 8 shows the mesh details of the Feijão dam model.

The dam construction, operation and post-closing stages were simulated using static analysis, with dynamic analysis used for simulating the catastrophic dam failure. The sequence of the Brumadinho tailings dam life cycle is presented in Fig. 9. For the construction modelling, details of each dam raising, such as the geometry change, layering characteristics of the coarse and fine tailings, and phreatic lines were reflected in the model. The stress and strain history during dam operation and construction stages were tracked. After the dam stopped receiving tailings wastes, the time-dependent behaviour of tailings was simulated with a particular focus on the progressive local failure evolving into the catastrophic global failure. At the onset of global failure, the dynamic analysis was switched on immediately.

Tailings are a three-phase material containing air, water and solid particles, and the response upon loading is influenced by the rate of accumulation and dissipation of interparticle pore water pressures. For a general long-term process, where negligible excess pore water pressures below and dry tailings above the phreatic surface could be assumed, an effective stress framework is used with tailings described by the Mohr-Coulomb constitutive law<sup>43</sup> with cohesion,  $c'$ , and internal frictional angle,  $\phi'$ . To account for material degradation during shearing<sup>44</sup>, the frictional angle is reduced from the peak,  $\phi'_p$ , towards the residual,  $\phi'_r$ , given by (see Fig. 8c):

$$\phi' = \max \left[ \phi'_p + \left( \phi'_r - \phi'_p \right) \frac{\gamma^{ie}}{\gamma_r^{ie}}, \phi'_r \right] \quad (1)$$

where  $\gamma^{ie}$  is the accumulated inelastic shear strain as a sum of plastic strain  $\gamma^p$  and creep strain  $\gamma^{cr}$ , and  $\gamma_r^{ie}$  is the value of  $\gamma^{ie}$  at the onset

of residual state. In fast processes such as during rapid discharge and brittle failure, where a favourable dissipation of pore pressures is impossible, we used a total stress framework with the peak undrained shear strength of tailings,  $s_{u,p}$ , defined via the vertical effective stress,  $\sigma'_v$ , as

$$s_{u,p} = k\sigma'_v \quad (2)$$

where  $k$  is the strength ratio affected by factors such as particle size and internal bond structure. With plastic shearing, the undrained shear strength is softening (see Fig. 8d)

$$s_u = \max \left[ s_{u,p} + \left( s_{u,r} - s_{u,p} \right) \frac{\gamma^{ie}}{\gamma_r^{ie}}, s_{u,r} \right] \quad (3)$$

where  $s_{u,r}$  is the residual shear strength.

The generalised Maxwell model<sup>45</sup>, also known as the Maxwell–Wiechert model, was adopted to simulate the creep behaviour of tailings. In this model, several Maxwell elements, each consisting of a spring and a dashpot, are assembled in parallel as shown in Fig. 8e. Given  $N + 1$  elements with shear modulus  $G_i$  and viscosity  $\eta_i$ , the time dependent shear modulus,  $G(t)$ , can be described by the Prony series

$$G(t) = G_0 \left[ 1 - \sum_{i=1}^N g_i (1 - e^{-t/\bar{\tau}_i}) \right] \quad (4)$$

$$\bar{\tau}_i = \frac{\eta_i}{G_i}, g_i = \frac{G_i}{G_0}$$

where  $G_0$  is the instantaneous modulus and  $g_i$  is the standardised modulus of Maxwell element.

Based on the laboratory test results reported by the panel<sup>18</sup>, the following parameters were adopted for the coarse tailings:

$$E = 50 \text{ MPa}, \nu = 0.3, c' = 2 \text{ kPa}, \phi'_p = 36^\circ, \phi'_r = 33^\circ, \gamma_r^{ie} = 4\%, k = 1.3, K_0 = 0.43;$$

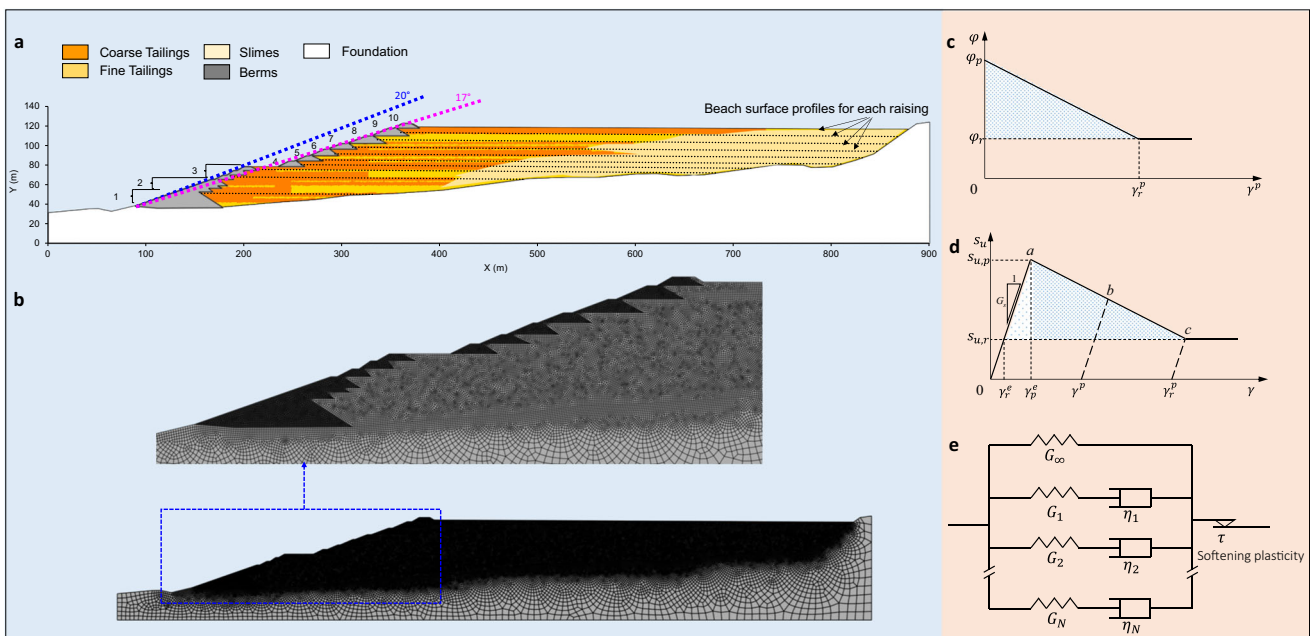


**Fig. 8 Numerical model of the Brumadinho tailings and Feijão dam.** **a** Layout of raisings and layering feature of tailings. **b** Mesh structure used in the numerical modelling. **c** Strain-controlled tailings softening of frictional angle. **d** Strain-controlled tailings softening of undrained strength. **e** The generalised Maxwell model with softening plasticity (the viscoelasticity is governed by the spring-dashpot system with spring and dashpot controlling elasticity and creep, respectively).

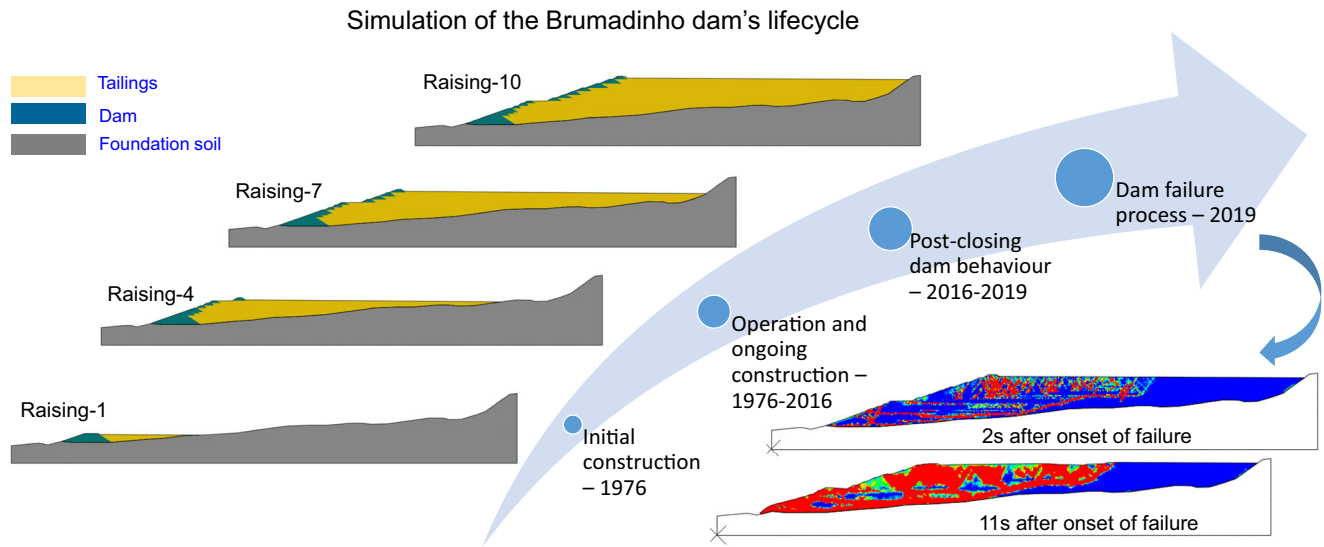


**Fig. 9 Programme for the whole-life modelling of the Feijão dam.** The program follows the entire evolution of the dam from construction and operation to post-closing performance and dynamic failure. Colours in the two dam models at the right bottom corner correspond to different shear strain levels indicated in Figs. 4, 5.

and fine tailings:

$$E = 50 \text{ MPa}, \nu = 0.3, c' = 2 \text{ kPa}, \varphi'_p = 33^\circ, \varphi'_r = 33^\circ, \gamma_r^{ie} = 4\%, k = 0.16, K_0 = 0.43.$$

Note that the Poisson's ratio,  $\nu$ , was set to 0.495 and the Young's modulus,  $E$ , to  $300s_{u,p}$  (see Eq. (2)) once undrained conditions were applied, which are common values for normally consolidated tailings. The sensitivity of tailings, which is the ratio of peak and residual undrained shear strengths, i.e.,  $S_t = s_{u,p}/s_{u,r}$ , was set to 5 which is well within the range obtained from lab tests. The total unit weight of tailings is  $26 \text{ kN/m}^3$  (Robertson et al.<sup>18</sup>). Parameters of the Prony series, i.e., Eq. (4), for the creep behaviour were determined by the best fit of experimental data from two triaxial tests with constant loads (Fig. 2d). Six Maxwell elements were used, with the instantaneous shear modulus of  $G_0 = 19.2 \text{ MPa}$  and the long-term shear modulus is  $G_\infty = 8.1 \text{ MPa}$ , resulting in a fit with the root mean square error less than 1%. The parameters for the foundation soils were adopted as:

$$E = 100 \text{ MPa}, \nu = 0.3, \varphi'_p = 38^\circ, \varphi'_r = 35^\circ, \gamma_r^{ie} = 6\%$$

with no creep considered. The total unit weight of foundation soils is  $22 \text{ kN/m}^3$  estimated based on reported dry unit weight and specific gravity. The values are common for compacted soils and were found to have little influence on the numerical results as the foundation remains stable during the whole process.

**Analytical criterion for the critical length of the slip surface.** From the numerical modelling (Fig. 5b) it can be concluded that the catastrophic slip surface growth commenced when the combined length of the top two surfaces reached the length of about 250 m. This result can be validated using the criterion for the onset of catastrophic slip surface growth in a cut planar slope<sup>36</sup>:

$$l_c = \frac{1-r}{r_0} l_u \quad (5)$$

$$r = \frac{\tau_g - s_{u,r}}{s_{u,p} - s_{u,r}}, l_u = \sqrt{\frac{E' h \delta_r}{s_{u,p} - s_{u,r}}}$$

where  $l_c$  is the critical length for the onset of catastrophic slip surface growth,  $r$  is the shear stress ratio representing the level of gravity shear stress ( $\tau_g$ ) at the tip of the slip surface;  $r_0$  is the averaged shear

stress ratio over the entire slip surface; and  $l_u$  is the characteristic length dependent on the properties of tailings ( $E'$  is the averaged plane strain elastic modulus of coarse tailings beaches above the slip surface and  $\delta_r$  is the plastic displacement reducing the strength to the residual state) and slip surface depth  $h$ . Similar to the numerical analysis, the following parameters were adopted:

$$E^{\text{coarse}} = 300s_{u,p}^{\text{coarse}}, \nu = 0.495; E' = \frac{E}{1-\nu^2}; h \approx 60 \text{ m}; \delta_r = 0.08 \text{ m};$$

$s_{u,p}^{\text{coarse}} = 1.3\sigma'_v; s_{u,p} = 0.16\sigma'_v; S_t = \frac{s_{u,p}}{s_{u,r}} = 5$ . The average vertical stress of coarse tailings beaches above the slip surface is about a half of the value at the slip surface, therefore the average peak undrained shear strength of the coarse tailings beach is about four times the value for fine tailings at the slip surface:  $s_{u,p}^{\text{coarse}} \approx 4s_{u,p}$ . It follows that for the two slip surfaces of major concern, the value of  $l_u$  can be estimated at 98 m. Measured from the numerical modelling, the average shear stress ratio within the slip surface is  $r_0 \approx 0.5$ , and the shear stress ratio at the slip surface tip is  $r \approx 0$ . This results in the critical length of slip surface of about 200 m, which is the same order of magnitude as the value measured from the numerical modelling.

Similar analysis was carried out for the bottom three surfaces (No. 3, 4, and 5 in Fig. 5b) which are also about to merge at the onset of the failure. The critical length of a slip surface at the depth of the bottom three surfaces (averaged at 70 m) is 210 m estimated based on Eq. (5), which is larger than the total length of the three merging surfaces (140 m). This is consistent with the observation that the catastrophic slip surface growth takes place after merging of the top two surfaces rather than of the three bottom ones.

**Data availability**

Site investigation and lab experimental data of Brumadinho tailings are from the expert panel report (organised by Vale S.A) at <http://www.b1technicalinvestigation.com/>. The Satellite images are taken from the Google Earth at <https://earth.google.com/web/>. Other data used in this study is publicly available at the Figshare repository <https://doi.org/10.6084/m9.figshare.24295045>.

**Code availability**

The finite element code with implementation of constitutive models into the Abaqus software is available upon request.

Received: 11 May 2023; Accepted: 6 November 2023;

Published online: 16 January 2024

## References

- Silva Rotta, L. H. et al. The 2019 Brumadinho tailings dam collapse: Possible cause and impacts of the worst human and environmental disaster in Brazil. *Int. J. Appl. Earth Obs. Geoinform.* **90**, 102119 (2020).
- Grebby, S. et al. Advanced analysis of satellite data reveals ground deformation precursors to the Brumadinho Tailings Dam collapse. *Commun. Earth Environ.* **2**, 1–9 (2021).
- Parente, C. E. et al. First year after the Brumadinho tailings' dam collapse: Spatial and seasonal variation of trace elements in sediments, fishes and macrophytes from the Paraopeba River, Brazil. *Environ. Res.* **193**, 110526 (2021).
- do Carmo, F. F. et al. Fundão tailings dam failures: the environment tragedy of the largest technological disaster of Brazilian mining in global context. *Perspect. Ecol. Conserv.* **15**, 145–151 (2017).
- dos Santos Vergilio, C. et al. Immediate and long-term impacts of one of the worst mining tailing dam failure worldwide (Bento Rodrigues, Minas Gerais, Brazil). *Sci. Total Environ.* **756**, 143697 (2021).
- Pegg, S. Mining and poverty reduction: Transforming rhetoric into reality. *J. Clean. Product* **14**, 376–387 (2006).
- Vick, S. G. *Planning, design, and analysis of tailings dams*. (BITech Publishers Ltd, 1990).
- Rico, M., Benito, G., Salgueiro, A. R., Díez-Herrero, A. & Pereira, H. G. Reported tailings dam failures: a review of the European incidents in the worldwide context. *J. Hazard. Mater.* **152**, 846–852 (2008).
- Hatje, V. et al. The environmental impacts of one of the largest tailing dam failures worldwide. *Sci. Rep.* **7**, 1–13. (2017).
- Owen, J. R., Kemp, D., Lèbre, É., Svobodova, K. & Murillo, G. P. Catastrophic tailings dam failures and disaster risk disclosure. *Int. J. Disaster Risk Reduct* **42**, 101361 (2020).
- Van Niekerk, H. J. & Viljoen, M. J. Causes and consequences of the Merriespruit and other tailings-dam failures. *Land Degrad. Dev.* **16**, 201–212 (2005).
- Coulibaly, Y., Belem, T. & Cheng, L. Numerical analysis and geophysical monitoring for stability assessment of the Northwest tailings dam at Westwood Mine. *Int. J. Mining Sci. Technol.* **27**, 701–710 (2017).
- Santamarina, J. C., Torres-Cruz, L. A. & Bachus, R. C. Why coal ash and tailings dam disasters occur. *Science* **364**, 526–528 (2019).
- Clarkson, L. & Williams, D. An overview of conventional tailings dam geotechnical failure mechanisms. *Mining. Metallurgy Explor.* **38**, 1305–1328 (2021).
- De Lima, R. E., de Lima Picanço, J., da Silva, A. F. & Acordes, F. A. An anthropogenic flow type gravitational mass movement: the Córrego do Feijão tailings dam disaster. *Brumadinho Brazil. Landslides* **17**, 2895–2906 (2020).
- Thompson, F. et al. Severe impacts of the Brumadinho dam failure (Minas Gerais, Brazil) on the water quality of the Paraopeba River. *Sci. Total Environ.* **705**, 135914 (2020).
- Ouellet, S. M., Dettmer, J., Olivier, G., DeWit, T. & Lato, M. Advanced monitoring of tailings dam performance using seismic noise and stress models. *Commun. Earth Environ.* **3**, 301 (2022).
- Robertson, P. K., de Melo, L., Williams, D. J. & Wilson, G. W. Report of the expert panel on the technical causes of the failure of Feijão Dam I. <http://www.b1technicalinvestigation.com/> (2020).
- Arroyo, M. and Gens, A., 2021. Computational Analyses of Dam I Failure at the Corrego de Feijao Mine in Brumadinho. Final Report for VALE S.A., August 2021.
- Wolff, A. P., da Costa, G. M. & de Castro Dutra, F. A comparative study of ultra-fine iron ore tailings from Brazil. *Mineral Proc. Extract. Metallurgy Rev.* **32**, 47–59 (2010).
- Schnaid, F., Bedin, J., Viana da Fonseca, A. J. P. & de Moura Costa Filho, L. Stiffness and strength governing the static liquefaction of tailings. *J. Geotech. Geoenviron. Engineer.* **139**, 2136–2144 (2013).
- Chen, Q. et al. Strength and deformation of tailings with fine-grained interlayers. *Engineer. Geology* **256**, 110–120 (2019).
- Jeyapalan, J. K., Duncan, J. M. & Seed, H. B. Investigation of flow failures of tailings dams. *J. Geotech. Engineer.* **109**, 172–189 (1983).
- Martin, T. E. & McRoberts, E. C. Some considerations in the stability analysis of upstream tailings dams. In *Proceedings of the sixth international conference on tailings and mine waste*, 99, 287–302. (Rotterdam, Netherlands: AA Balkema, 1999).
- Whittle, A. J., El-Naggar, H. M., Akl, S. A. & Galaa, A. M. Stability analysis of upstream tailings dam using numerical limit analyses. *J. Geotech. Geoenviron. Engineer.* **148**, 04022035 (2022).
- Freund, L. B. The mechanics of dynamic shear crack propagation. *J. Geophys. Res: Solid Earth* **84**, 2199–2209 (1979).
- Hillerborg, A., Modéer, M. & Petersson, P. E. Analysis of crack formation and crack growth in concrete by means of fracture mechanics and finite elements. *Cement Concrete Res.* **6**, 773–781 (1976).
- Palmer, A. C. & Rice, J. R. The growth of slip surfaces in the progressive failure of over-consolidated clay. *Proc. Royal Soc. London. A. Mathe Phys. Sci.* **332**, 527–548 (1973).
- Puzrin, A. M. & Germanovich, L. N. The growth of shear bands in the catastrophic failure of soils. *Proc. Royal Soc. A: Mathe. Phys. Engineer. Sci.* **461**, 1199–1228 (2005).
- Puzrin, A. M., Faug, T. & Einav, I. The mechanism of delayed release in earthquake-induced avalanches. *Proc. Royal Soc. A* **475**, 20190092 (2019).
- Gaume, J. & Puzrin, A. M. Mechanisms of slab avalanche release and impact in the Dyatlov Pass incident in 1959. *Commun. Earth Environ* **2**, 1–11 (2021).
- E. E. Alonso, N. M. Pinyol & A. M. Puzrin. Earth Dam Sliding Failure: Aznalcollar Dam, Spain in *Geomechanics of Failures: Advanced Topics*, 130–164 (Dordrecht: Springer, 2010).
- Zhang, W., Klein, B., Randolph, M. F. & Puzrin, A. M. Upslope failure mechanisms and criteria in submarine landslides: Shear band propagation, slab failure and retrogression. *J. Geophys. Res: Solid Earth* **126**, e2021JB022041 (2021).
- Gibson, R. E. The progress of consolidation in a clay layer increasing in thickness with time. *Geotechnique* **8**, 171–182 (1958).
- Puzrin, A. Piping Criteria for Hydraulically Stable Anisotropic Slopes. *J. Geotech. Geoenviron. Engineer* **147**, 04021129 (2021).
- Zhang, W., Wang, D., Randolph, M. F. & Puzrin, A. M. Catastrophic failure in planar landslides with a fully softened weak zone. *Géotechnique* **65**, 755–769 (2015).
- Ligier, P. L. Implementation of non-Newtonian rheological models in TELEMAC-2D. In Online proceedings of the papers submitted to the 2020 TELEMAC-MASCARET User Conference October 2020 (14–25).
- Lumbroso, D., Davison, M., Body, R. & Petkoveš, G. Modelling the Brumadinho tailings dam failure, the subsequent loss of life and how it could have been reduced. *Nat. Hazards Earth Syst Sci* **21**, 21–37 (2021).
- Tsai, T. L. & Wang, J. K. Examination of influences of rainfall patterns on shallow landslides due to dissipation of matric suction. *Environ. Earth Sci.* **63**, 65–75 (2011).
- Loubere, R., Maire, P. H., Shashkov, M., Breil, J. & Galera, S. ReALE: a reconnection-based arbitrary-Lagrangian–Eulerian method. *J. Comput. Phys.* **229**, 4724–4761 (2010).
- Perić, D., Owen, D. R. J. & Honnor, M. A model for finite strain elasto-plasticity based on logarithmic strains: Computational issues. *Comput. Methods. Appl. Mech. Engineer* **94**, 35–61 (1992).
- Dassault Systèmes. *Abaqus 2020 documentation* (Dassault Systèmes Simulia Corp, Providence, RI, USA, 2020).
- Sloan, S. W. & Booker, J. R. Removal of singularities in Tresca and Mohr–Coulomb yield functions. *Commun. Appl. Numer. Methods* **2**, 173–179 (1986).
- Wang, Z. L., Li, Y. C. & Wang, J. G. A damage-softening statistical constitutive model considering rock residual strength. *Comput. Geosci* **33**, 1–9 (2007).
- Park, S. W. & Schapery, R. Methods of interconversion between linear viscoelastic material functions. Part I—A numerical method based on Prony series. *Int. J. Solids Struct* **36**, 1653–1675 (1999).

## Acknowledgements

The authors would like to thank Dr. Victor Sakano (University of Sao Paulo) for valuable discussions on the topic.

## Author contributions

F.Z. collected the data, developed the code, ran all the simulations, conducted the data analysis and visualisation. W.Z. performed analytical modelling and assisted with numerical simulation. A.M.P. conceived the key idea of the study and as the project leader provided funding, technical and programmatic oversight. F.Z. drafted the manuscript and all authors contributed to manuscript revision.

## Competing interests

The authors declare no competing interests.

**Additional information**

**Supplementary information** The online version contains supplementary material available at <https://doi.org/10.1038/s43247-023-01086-9>.

**Correspondence** and requests for materials should be addressed to Alexander M. Puzrin.

**Peer review information** *Communications Earth & Environment* thanks the anonymous reviewers for their contribution to the peer review of this work. Primary Handling Editors: Joe Aslin and Carolina Ortiz Guerrero. A peer review file is available.

**Reprints and permission information** is available at <http://www.nature.com/reprints>

**Publisher's note** Springer Nature remains neutral with regard to jurisdictional claims in published maps and institutional affiliations.



**Open Access** This article is licensed under a Creative Commons Attribution 4.0 International License, which permits use, sharing, adaptation, distribution and reproduction in any medium or format, as long as you give appropriate credit to the original author(s) and the source, provide a link to the Creative Commons licence, and indicate if changes were made. The images or other third party material in this article are included in the article's Creative Commons licence, unless indicated otherwise in a credit line to the material. If material is not included in the article's Creative Commons licence and your intended use is not permitted by statutory regulation or exceeds the permitted use, you will need to obtain permission directly from the copyright holder. To view a copy of this licence, visit <http://creativecommons.org/licenses/by/4.0/>.

© The Author(s) 2024